Copy 215
RM A52D29

53-28-61

NACA

RESEARCH MEMORANDUM

COMPARISON BETWEEN PREDICTION AND EXPERIMENT FOR

ALL-MOVABLE WING AND BODY COMBINATIONS AT

SUPERSONIC SPEEDS - LIFT, PITCHING

MOMENT, AND HINGE MOMENT

By Jack N. Nielsen, George E. Kaattari, and
William C. Drake

Ames Aeronautical Laboratory
Moffett Field, Calif.

NATIONAL ADVISORY COMMITTEE
FOR AERONAUTICS

WASHINGTON
August 8, 1952

NATIONAL ADVISORY COMMITTEE FOR AERONAUTICS

RESEARCH MEMORANDUM

COMPARISON BETWEEN PREDICTION AND EXPERIMENT FOR

ALL-MOVABLE WING AND BODY COMBINATIONS AT

SUPERSONIC SPEEDS — LIFT, PITCHING

MOMENT, AND HINGE MOMENT

By Jack N. Nielsen, George E. Kaattari, and
William C. Drake

SUMMARY

A simple method is presented for estimating lift, pitching-moment, and hinge-moment characteristics of all-movable wings in the presence of a body as well as the characteristics of wing-body combinations employing such wings. In general, good agreement between the method and experiment was obtained for the lift and pitching moment of the entire wing-body combination and for the lift of the wing in the presence of the body. The method is valid for moderate angles of attack, wing deflection angles, and width of gap between wing and body.

The method of estimating hinge moment was not considered sufficiently accurate for triangular all-movable wings. An alternate procedure is proposed based on the experimental moment characteristics of the wing alone. Further theoretical and experimental work is required to substantiate fully the proposed procedure.

INTRODUCTION

The use of all-movable wings for controlling missiles has become important not only for canard missiles but also for conventional tail-aft missiles. Under the limitations of the restricted spans usually permissible for missiles, the use of all-movable controls rather than flap-type controls enables the designer to obtain more control area and greater effectiveness. While controls of triangular plan form can have small hinge moments over the restricted Mach number range anticipated in the tactical use of some air-to-air missiles, other plan forms may also yield small hinge moments.

Although some data are available on the effectiveness of all-movable controls in supersonic flow, relatively few data are available on hinge moments. In reference 1, Conner has shown that on a wing and body combination the lift effectiveness associated with angle of attack is greater than that associated with wing deflection angle by an amount in agreement with that predicted by upwash theory. In reference 2, Stone has shown that an all-movable delta control can have small hinge moments in the Mach number range 0.7 to 1.4. The importance of triangular control surfaces for operation through the transonic range is thus clear. Concerning the effects of gaps on control characteristics, little is known, particularly for large control deflections.

While some experimental information on all-movable controls is available, no comprehensive theory for the aerodynamic characteristics of these controls has yet been advanced. It is the purpose of this report to present a simple method for determining the aerodynamic characteristics of all-movable controls mounted on circular bodies and of the wing-body combinations employing these controls and to compare the predicted results with those from experiment.

This report represents the first of two reports; it treats the subjects of lift, pitching moment, and hinge moment, and the second report considers drag due to lift and lift-drag ratio.

SYMBOLS

A $\qquad$ aspect ratio of exposed wing panels joined together

c $\qquad$ chord of wing at any spanwise position, inches

$\bar{c}$ $\qquad$ mean aerodynamic chord $\left(\dfrac{\int_r^s c^2 dy}{\int_r^s c\ dy} \right)$, inches

C_h $\qquad$ hinge-moment coefficient $\left(\dfrac{H}{q S_W \bar{c}} \right)$

C_{h_α} $\qquad$ rate of change of hinge-moment coefficient with angle of attack $\left(\dfrac{\partial C_h}{\partial \alpha} \right)$, per radian

C_{h_δ} rate of change of hinge-moment coefficient with wing deflection $\left(\dfrac{\partial C_h}{\partial \delta}\right)$, per radian

C_L lift coefficient $\left(\dfrac{L}{qS_W}\right)$

C_{L_α} lift-curve slope for angle of attack $\left(\dfrac{\partial C_L}{\partial \alpha}\right)$, per radian

C_{L_δ} lift-curve slope for wing deflection angle $\left(\dfrac{\partial C_L}{\partial \delta}\right)$, per radian

$\left(C_{L_\alpha}\right)_W$ lift-curve slope due to angle of attack of wing alone, per radian

C_m pitching-moment coefficient about body nose $\left(\dfrac{M}{qS_W \bar{c}}\right)$

C_{m_α} pitching-moment-curve slope for angle of attack $\left(\dfrac{\partial C_m}{\partial \alpha}\right)$, per radian

C_{m_δ} pitching-moment-curve slope for wing deflection angle $\left(\dfrac{\partial C_m}{\partial \delta}\right)$, per radian

c_r chord at wing-fuselage juncture, inches

c_t chord at wing tip, inches

d body diameter, inches

g gap between wing and body, inches

H hinge moment, pound-inches

$k_{B(W)}$ $\dfrac{L_{B(W)}}{L_W}$ for zero angle of attack and varying wing deflection angle

$k'_{B(W)}$ approximate value of $k_{B(W)}$

$k_{W(B)}$ $\dfrac{L_{W(B)}}{L_W}$ for zero angle of attack and varying wing deflection angle

$K_{B(W)}$ $\dfrac{L_{B(W)}}{L_W}$ for zero wing deflection angle and varying angle of attack

$K_{W(B)}$ $\dfrac{L_{W(B)}}{L_W}$ for zero wing deflection angle and varying angle of attack

K_N $\dfrac{L_N}{L_W}$

l body length, inches

$\bar{l}$ distance from forward end of body to center of pressure of wing-body combination, inches

l_f length from forward end of body to leading edge of wing-body juncture, inches

$\bar{l}_N$ distance from forward end of body to nose center of pressure, inches

l_a distance from base of body to trailing edge of wing-body juncture, inches

L lift force, pounds

m cotangent of leading-edge sweep angle

M pitching moment, pound-inches

M_O free-stream Mach number

Δp static pressure difference between top and bottom of wing, pounds per square inch

$\left(\dfrac{\Delta p}{q\delta}\right)_W$ wing loading due to unit wing deflection angle

q free-stream dynamic pressure, pounds per square inch

r radius of cylindrical portion of body, inches

R Reynolds number based on mean aerodynamic chord of exposed wing panel unless otherwise stated

s semispan of wing-body combination, inches

S_W area of exposed wing panels joined together, square inches

x,y   Cartesian coordinates

V   volume of body assuming body cross section uniform behind
           position of maximum cross section, cubic inches

V_o free-stream velocity, inches per second

$\left(\dfrac{\bar{x}}{c_r}\right)$ distance from leading edge of wing-body juncture to center
           of pressure in fraction of wing root chord

$\left(\dfrac{x}{c_r}\right)_H$ distance from leading edge of wing-body juncture to hinge
           line in fraction of wing root chord

α angle of attack, radians

β $\sqrt{M_o{}^2 - 1}$

βA effective aspect ratio

$(\beta A)^*$ critical effective aspect ratio

δ wing deflection angle, radians

Λ leading-edge sweep angle, degrees

λ wing taper ratio $\left(\dfrac{c_t}{c_r}\right)$

τ radius-semispan ratio $\left(\dfrac{r}{s}\right)$

Subscripts

N   body nose

W   wing alone

W(B)   wing in presence of body

B(W)   body in presence of wing exclusive of nose

C   wing-body combination

α α variable, δ constant

δ δ variable, α constant

C_α wing-body combination and α variable, δ constant

        Other compound subscripts to be interpreted similarly to the
preceding compound subscript

THEORETICAL CONSIDERATIONS

        The theory developed here is for wing-body combinations at zero
angle of bank and for no gap between the wing and body. The use of no-
gap theory is dictated by the fact that the experimental results for
configurations with gaps are in good accord with no-gap theory, as will
subsequently be shown. The present method is a mixture of slender-body
theory and linear theory, and as such is valid only over the ranges of
angle of attack and wing deflection angle for which the characteristics
vary linearly.

        A theoretical method is presented for determining the values of
C_{L_α} and C_{L_δ} for wing-body combinations and for the wing in the presence
the body. Also a method is presented for estimating C_{m_α} and C_{m_δ} for
the combination, or what is equivalent, the centers of pressure for
variations of α and δ. The available theory for the estimation of
hinge moments for triangular and rectangular wings is summarized. The
results are given in terms of certain dimensionless lift and distance
ratios together with the lift-curve slope of the wing alone. For the
purposes of this report the wing alone is defined to be the exposed wing
panels joined together.

        Most complete missile configurations possess two sets of lifting
surfaces, wings and tails, either of which may be all-movable. Inter-
ference between wing and tail influences the effectiveness of an all-
movable control; for this reason the characteristics of the combinations,
C_{L_α}, C_{L_δ}, C_{m_α}, and C_{m_δ}, determined by the method of this report apply
only to combinations having one set of lifting surfaces.

Lift Effectiveness

        <u>Angle of attack</u>.- A method that has proven valid for estimating the
value of C_{L_α} for a combination with no gap is presented in reference 3.
This method is applied in this report to combinations having a gap.
Attention is restricted for the present to the case for which the diam-
eter is uniform along the winged part of the body, but the case of
nonuniform diameter will subsequently be discussed. The lift acting on

the nose[1] of the body alone, the lift acting on the wing in the presence of the body, and the lift acting on the body due to the addition of the wing are defined by the parameters K_N, $K_{W(B)}$, and $K_{B(W)}$ as follows:

$$K_N = \frac{L_N}{L_W} \tag{1}$$

$$K_{W(B)} = \frac{L_{W(B)}}{L_W} \qquad \text{with } \delta = 0 \tag{2}$$

$$K_{B(W)} = \frac{L_{B(W)}}{L_W} \qquad \text{with } \delta = 0 \tag{3}$$

where the reference lift L_W is the lift of the wing alone. From these definitions it follows that

$$\left(C_{L_\alpha}\right)_C = \left[K_N + K_{W(B)} + K_{B(W)}\right] \left(C_{L_\alpha}\right)_W \tag{4}$$

where $\left(C_{L_\alpha}\right)_W$ is the wing-alone lift-curve slope. The value of $\left(C_{L_\alpha}\right)_W$ from experiment should be used if available, otherwise the value from linear theory can be used.

According to equation (4) the problem of obtaining $\left(C_{L_\alpha}\right)_C$ depends on obtaining values of K_N, $K_{W(B)}$, and $K_{B(W)}$. The values of K_N obtained by slender-body theory,

$$K_N = \frac{2\pi r^2}{S_W \left(C_{L_\alpha}\right)_W} \tag{5}$$

are used throughout this report. A chart for obtaining $K_{W(B)}$, as given by slender-body theory, was presented in reference 3 and is reproduced as figure 1 of this report. If the aspect ratio is sufficiently low that the wing-tip Mach cones intersect the wing-body juncture in front of the trailing edge, then the slender-body-theory value of $K_{B(W)}$ as given by figure 1 is to be used. The effective aspect ratio (βA) below which slender-body theory is to be used is given by

$$(\beta A)^* = \frac{4}{(1 + \lambda)\left(\frac{1}{\beta m} + 1\right)}$$

---

[1]The nose of the body is that part of the body in front of the leading edge of the wing-body juncture for cases wherein the diameter is uniform along the winged part of the body. It is further assumed for purpose of computation that the lift of the body alone is confined to the body nose.

This result was derived on the assumption that the wing panel is trape-
zoidal. For values of $\beta A > (\beta A)^*$ an alternate method of determining
$K_{B(W)}$ was given in reference 3. For this case, $K_{B(W)}$ can be determined
from the design chart[2] of figure 2.

It is clear from the definition of the parameter $K_{W(B)}$ that the
lift-curve slope of the exposed wing in the presence of the body is

$$\left(C_{L_\alpha}\right)_{W(B)} = K_{W(B)} \left(C_{L_\alpha}\right)_W \tag{6}$$

Wing deflection angle.- The method for estimating the values of
C_{L_δ} for the combination and for the wing in the presence of the body is
analogous to the method for C_{L_α}. Two parameters are defined in the
following equations:

$$k_{W(B)} = \frac{L_{W(B)}}{L_W} \qquad \text{with } \alpha = 0 \tag{7}$$

$$k_{B(W)} = \frac{L_{B(W)}}{L_W} \qquad \text{with } \alpha = 0 \tag{8}$$

From these definitions it follows readily that

$$\left(C_{L_\delta}\right)_C = \left[k_{W(B)} + k_{B(W)} \right] \left(C_{L_\alpha}\right)_W \tag{9}$$

and

$$\left(C_{L_\delta}\right)_{W(B)} = k_{W(B)} \left(C_{L_\alpha}\right)_W \tag{10}$$

According to equations (9) and (10), the problem of determining
C_{L_δ} is equivalent to that of obtaining values of $k_{W(B)}$ and $k_{B(W)}$.
There are several solutions available for determining $k_{W(B)}$, slender-
body theory for slender triangular wing and body combinations, and an

---

[2]This design chart was originally intended for use with wings having
triangular, rectangular, or trapezoidal panels. However, the chart
can be used for wing panels having trailing edges that are not straight
by using an equivalent taper for λ. This taper is that of the equiva-
lent trapezoidal wing panel having the same span, root chord, and area
as the given panel.

exact linear theory solution for rectangular wing and body combinations. The slender-body result based on an unpublished solution of Gaynor J. Adams of the Ames Aeronautical Laboratory for the wing loading (see appendix) gives the following expression for $k_{W(B)}$ in terms of τ, the radius-semispan ratio.

$$k_{W(B)} = \frac{1}{\pi}\left[\frac{\pi^2}{4}\frac{(\tau+1)^2}{\tau^2} + \frac{\pi(\tau^2+1)^2}{\tau^2(\tau-1)^2}\sin^{-1}\frac{\tau^2-1}{\tau^2+1} - \frac{2\pi(\tau+1)}{\tau(\tau-1)} + \right.$$

$$\frac{(\tau^2+1)^2}{\tau^2(\tau-1)^2}\left(\sin^{-1}\frac{\tau^2-1}{\tau^2+1}\right)^2 - \frac{4}{\tau}\frac{(\tau+1)}{(\tau-1)}\sin^{-1}\frac{\tau^2-1}{\tau^2+1} + $$

$$\left.\frac{8}{(\tau-1)^2}\log\frac{\tau^2+1}{2\tau}\right] \tag{11}$$

The value of $k_{W(B)}$ so obtained is presented in figure 1 and is strictly applicable only to slender wing-body combinations. The exact linear-theory results for rectangular wing and body combinations, taken from reference 4, are presented in figure 3 where they are compared with the preceding slender-body results. There is generally a small difference between the two predictions, never exceeding about 10 percent for values of βA of 2 or greater. When rectangular wings of effective aspect ratio 2 or greater are involved, then the linear-theory values of $k_{W(B)}$ should be used. For the range of βA between 0 and 2 linear-theory results for $k_{W(B)}$ are not available. However, as βA approaches zero the rectangular wing and body combination becomes more slender, until at $\beta A = 0$ slender-body theory is exact for the combination. On the basis of these considerations it was decided to use $k_{W(B)}$ as given by slender-body theory for all rectangular wing and body combinations with $\beta A < 2$.

The only general method for determining $k_{B(W)}$ is slender-body theory. It has been shown in reference 5 by use of a reciprocal theorem that for combinations with cylindrical bodies the following equality is valid under the assumptions of slender-body theory:

$$k_{B(W)} = K_{W(B)} - k_{W(B)} \tag{12}$$

The values of $k_{B(W)}$ as given by equation (12) are included in figure 1, and this figure has been used for determining $k_{B(W)}$ throughout this report.

An interesting approximation that gives some insight into the interrelationships between $K_{B(W)}$, $K_{W(B)}$, $k_{B(W)}$, and $k_{W(B)}$ can be made. Assuming that the wing transmits a certain fraction of its lift to the

body irrespective of whether the lift is developed by angle of attack or wing deflection, an approximate value for $k_{B(W)}$, namely, $k'_{B(W)}$, is

$$k'_{B(W)} = k_{W(B)} \frac{K_{B(W)}}{K_{W(B)}} \tag{13}$$

The values of $k_{B(W)}$ and $k'_{B(W)}$ as determined from equations (12) and (13) do not differ by more than 0.01, a quantity that is practically indistinguishable in figure 1. This small difference is due to the difference in the forms of the load distribution on the wing for lifts due to angle of attack and wing deflection angle.

Moment Effectiveness

The moment effectiveness of an all-movable control can be measured by the quantities C_{m_α} and C_{m_δ} for the complete configuration. With the foregoing results for C_{L_α} and C_{L_δ}, finding C_{m_α} and C_{m_δ} is equivalent to obtaining $(\bar{l}/l)_\alpha$ and $(\bar{l}/l)_\delta$, the center-of-pressure positions for the complete combination.

Angle of attack.- A method for obtaining the value of C_{m_α} for the complete combination has been presented in reference 6. In this reference the basic equation given for C_{m_α} is

$$C_{m_\alpha} = \left[\frac{K_N \bar{l}_N + K_{W(B)} \bar{l}_{W(B)\alpha} + K_{B(W)} \bar{l}_{B(W)\alpha}}{\bar{c}} \right] \left(C_{L_\alpha} \right)_W \tag{14}$$

In this equation the reference length has been taken as the mean aerodynamic chord and the moments are about the body nose. The methods for determining K_N, $K_{W(B)}$, and $K_{B(W)}$ have already been discussed, and the methods given in reference 6 for obtaining the moment arms are now considered. The length $\bar{l}_N$ is found from slender-body theory as

$$\bar{l}_N = l \left(1 - \frac{V}{\pi r^2 l} \right) \tag{15}$$

where V is the volume of the body neglecting boattailing, that is, assuming the body to have a constant cross section behind the position of maximum cross section.

The values of $\bar{l}_{W(B)\alpha}$ can be determined from the following equation from a knowledge of $(\bar{x}/c_r)_{W(B)\alpha}$:

$$\bar{l}_{W(B)\alpha} = l_f + c_r\,(\bar{x}/c_r)_{W(B)\alpha} \qquad (16)$$

No general method for obtaining $(\bar{x}/c_r)_{W(B)\alpha}$ exists. In reference 6 it was pointed out that $(\bar{x}/c_r)_W$ was a good approximation to $(\bar{x}/c_r)_{W(B)\alpha}$, and this approximation has been used throughout this report except for triangular wing and body combinations. For triangular wing and body combinations a somewhat better value of $(\bar{x}/c_r)_{W(B)\alpha}$ can be obtained by using slender-body theory since this theory takes into account the interference. These results, taken from reference 6, are presented in figure 4. It is seen that the maximum deviation between the slender-body value and the wing-alone value of 0.667 is about 2 percent of the root chord. For the purposes of obtaining C_{m_α} for the entire combination this difference may not be significant. However, the difference may be significant in determining hinge moments. The value of $\bar{l}_{B(W)\alpha}$ for equation (14) is given in terms of $(\bar{x}/c_r)_{B(W)\alpha}$ by

$$\bar{l}_{B(W)\alpha} = l_f + c_r(\bar{x}/c_r)_{B(W)\alpha} \qquad (17)$$

A special chart for estimating the value of $(\bar{x}/c_r)_{B(W)\alpha}$ was given in reference 6 and is reproduced here as figure 5. These results are for a combination with an afterbody. Thus the values of the parameters in equation (14) can all be estimated and C_{m_α} calculated.

Wing deflection angle.- The determination of the moment effectiveness parameter C_{m_δ} can be obtained in a manner similar to that for C_{m_α}. The basic equation for C_{m_δ} is

$$C_{m_\delta} = \left[\frac{k_{W(B)}\ \bar{l}_{W(B)\delta} + k_{B(W)}\ \bar{l}_{B(W)\delta}}{\bar{c}}\right]\left(C_{L_\alpha}\right)_W \qquad (18)$$

The determinations of $k_{W(B)}$ and $k_{B(W)}$ have already been considered. The value of $\bar{l}_{W(B)\delta}$ is given in terms of $(\bar{x}/c_r)_{W(B)\delta}$ as

$$\bar{l}_{W(B)\delta} = l_f + c_r\,(\bar{x}/c_r)_{W(B)\delta} \qquad (19)$$

No general method for estimating $(\bar{x}/c_r)_{W(B)\delta}$ exists, but specialized

results are available for rectangular wing and body combinations for which $\beta A \geq 2$ or for slender triangular wing and body combinations. For the rectangular wing and body combinations, values of $(\bar{x}/c_r)_{W(B)\delta}$

based on linear theory obtained from reference 4 are presented in figure 6. The values of $(\bar{x}/c_r)_{W(B)\delta}$ are lower than the wing-alone

values by a few percent of the root chord. The results for slender triangular wing and body combinations as determined from slender-body theory in the appendix are shown in figure 4. The deviation of $(\bar{x}/c_r)_{W(B)\delta}$ from the wing-alone value of two-thirds is only a fractional

percent of the root chord. For the combination to which they apply, the results of figures 4 and 6 are to be used. For other combinations, $(\bar{x}/c_r)_W$ provides a good approximation to $(\bar{x}/c_r)_{W(B)\delta}$ until more accurate values are available.

The value of $\bar{l}_{B(W)\delta}$ for equation (18) is given in terms of $(\bar{x}/c_r)_{B(W)\delta}$ as

$$\bar{l}_{B(W)\delta} = l_f + c_r \, (\bar{x}/c_r)_{B(W)\delta} \tag{20}$$

A method for estimating $(\bar{x}/c_r)_{B(W)\alpha}$ was advanced in reference 6. If

the assumption is made that the center of pressure of the lift transferred from the wing to the body is not sensitive to whether the lift is developed by angle of attack or by wing deflection, there is no appreciable difference between $(\bar{x}/c_r)_{B(W)\alpha}$ and $(\bar{x}/c_r)_{B(W)\delta}$. Then figure 5 can

be used to estimate $(\bar{x}/c_r)_{B(W)\delta}$. Methods have thus been given for esti-

mating all the quantities in equation (18) for $C_{m\delta}$.

Hinge-Moment Coefficients

The methods for estimating $C_{m\alpha}$ and $C_{m\delta}$ for the complete combination contain within themselves the methods for obtaining $C_{h\alpha}$ and $C_{h\delta}$. However, it should be pointed out that, in general, greater accuracy is needed in the value of $(\bar{x}/c_r)_{W(B)}$ for estimating hinge moments than for

estimating the moment characteristics of the complete combination. Consider, for instance, a triangular all-movable control which has a nearly constant center-of-pressure position through the speed range, and

the hinge line of which is located close to the center-of-pressure location. For such a control, small changes in center-of-pressure position represent large changes in hinge-moment coefficient so that accurate values of $(\bar{x}/c_r)_{W(B)}$ are desired.

The values of C_{h_α} and C_{h_δ} are given very simply by the following expressions:

$$C_{h_\alpha} = (c_r/\bar{c}) \; K_{W(B)} \left[(\bar{x}/c_r)_{W(B)\alpha} - (x/c_r)_H \right] \left(C_{L_\alpha} \right)_W \quad (21)$$

$$C_{h_\delta} = (c_r/\bar{c}) \; k_{W(B)} \left[(\bar{x}/c_r)_{W(B)\delta} - (x/c_r)_H \right] \left(C_{L_\alpha} \right)_W \quad (22)$$

wherein the coefficients are based on the mean aerodynamic chord as the reference length. For triangular wing and body combinations the values of $(\bar{x}/c_r)_{W(B)\alpha}$ and $(\bar{x}/c_r)_{W(B)\delta}$ can be obtained from figure 4, and for rectangular wing and body combinations $(\bar{x}/c_r)_{W(B)\delta}$ can be obtained from figure 6. The foregoing methods for estimating hinge-moment coefficients, while they represent the best knowledge available at the present time, are not adequate as will be pointed out.

Effects of Gap and Nonuniform Body Diameter

The effects of gap between wing and body and of nonuniform body diameter need clarification. It is possible, on the basis of inviscid fluid theory, to calculate theoretically the effect of the gap on the lift of a wing-body combination. For instance, using the method of Lomax and Byrd in reference 7, the effect of a uniform gap can be determined on the assumptions that the wing has no thickness and that the wing boundary conditions can be specified on the horizontal plane passing through the body axis. On the basis of these assumptions large losses of lift due to the gap are indicated when compared to the no-gap solution of Spreiter in reference 8. However, these large losses are not found experimentally. While some of the losses predicted theoretically may be the result of an oversimplification of the inviscid fluid model, nevertheless it appears probable that some of the predicted losses are overcome by viscosity.

The case of a wing mounted on a body section of uniform diameter has been considered in the analysis. However, if the wing is mounted on a body section of variable diameter, as may well be the case for a canard surface, an approximate treatment of the problem can be made. First, the nose of the body is taken as that part of the body in front of the position of maximum thickness in determining K_N. In the determination

of $K_{B(W)}$ and $K_{W(B)}$ from figures 1 and 2, an average radius of the section of the body on which the wing is mounted should be used.

RESULTS AND DISCUSSION

The experimental lift, pitching-moment, and hinge-moment character-istics for a number of wing-body combinations employing all-movable wings have been analyzed and compared with the predictions of the simple method of this report. The geometric characteristics of the combina-tions are summarized in table I, and the experimental and theoretical values of the aerodynamic parameters for the combinations are also summarized in the table. The data are taken from references 1 and 9 to 18. Where no values are given for the width of gap between wing and body, these were not given in the references.

Lift Effectiveness

Angle of attack.- Before comparing the experimental values of $(C_{L_\alpha})_C$, which include the effects of gaps, with the theory for no gap, it is desirable to show that the losses of lift due to the gap predicted on the basis of inviscid fluid theory do not materialize. For this purpose the model numbered 10 in table I was tested with a variable gap and the results of the tests are shown in figure 7. The difference in lift-curve slope, $(C_{L_\alpha})_C$ exhibited between the case for $g/\sim = 0$ and g/s = 0.033 amounts only to about 2 percent. The g/s ratio of 0.033 corresponded to a gap of 3/32 inch on the model. For most of the angle-of-attack range during the tests of this model the boundary layer was laminar and, at zero angle of attack, was estimated to be about 1/32 inch in thickness at the wing leading edge. Thus the gap was of several boundary-layer thicknesses. While the effects of gap on lift have been shown to be unimportant, the effects on hinge moments may be considerable. Further data on this point are required.

The theoretical values of $(C_{L_\alpha})_C$ have been computed from equation (4) for the combinations of the table and the theoretical and experimental values are listed together in the table. These values are compared in figure 8(a), wherein the line of perfect agreement indicates exact correlation. All of the combinations, of which there are approximately 20, exhibit good agreement between theory and experiment. It appears, therefore, that the value of $(C_{L_\alpha})_C$ for a model with a gap of moderate proportions can be satisfactorily estimated from the no-gap theory of

this report. The theory would not be expected to apply for gaps which are very large compared to the boundary-layer thickness or for the nonlinear range of the lift curve.

The lift on the exposed wing panels of the wing-body combination has been measured for a number of combinations, as shown by the table. Comparison between the theoretical and experimental values of $(C_{L_\alpha})_{W(B)}$ is made in figure 8(b). It is seen from the figure that the theoretical and experimental values are in good accord except for a group of four points which is enclosed by a dashed line. These four points correspond to configurations utilizing small canard-type fins. While it is considered probable that the deviation between experiment and theory is the result of the very low Reynolds numbers for these fins as shown in table I, the possibility of erroneous experimental results cannot be precluded. Also shown in the figure are three points with flags. These are the three points for which the experimental values of $(C_{L_\alpha})_W$ are available. If in equation (6) the experimental values of $(C_{L_\alpha})_W$ are used instead of the values given by linear theory in obtaining $(C_{L_\alpha})_{W(B)}$, these points move into good correlation as shown by the solid points of figure 8(b). It appears, therefore, that the experimental values of $(C_{L_\alpha})_{W(B)}$ are predicted satisfactorily by the no-gap theory of this report except possibly for very low Reynolds numbers, very high angles of attack, or very large gaps.

Wing deflection angle.- The effects of wing deflection angle on lift have been studied in a manner similar to the effects for angle of attack. The theoretical values of $(C_{L_\delta})_C$ have been computed from equation (9) for all combinations of the table. Comparison is made between the experimental and theoretical values of $(C_{L_\delta})_C$ in figure 8(c). Careful examination must be given to the data of this figure before any conclusions are drawn. First, the data corresponding to the canard fins at low Reynolds numbers have been enclosed as in figure 8(b). They show about 80 percent of the theoretical values in this case. A group of three combinations corresponding to flagged symbols for which the wing-alone experimental values of $(C_{L_\alpha})_W$ are available are also indicated in figure 8(c). If, for the same combinations, the theoretical values of $(C_{L_\delta})_C$ are based on the experimental values of the wing-alone lift-curve slope, then the flagged points of figure 8(c) become the flagged solid points which are in very good correlation with experiment. Generally the predicted values of $(C_{L_\delta})_C$ tend to be somewhat too large for the data correlated. There are not sufficient data to determine whether this effect is due to inaccuracies in the theory or to a tendency of the experimental wing-alone lift-curve slopes to be less than the theoretical slopes.

A fundamental difference in the wing-body gap occurs between variations of α and δ. As δ increases the gap between wing and circular-cylindrical body increases for points not at the hinge line, and it might be expected that the increased gap causes an increased loss of lift. However, if on a percentage basis the loss of lift due to the gap increases as δ increases, then the variation of C_L as a function of δ should be nonlinear and of decreased slope. Only at angles of δ of roughly 10° or greater, depending on Mach number and aspect ratio, were nonlinearities observed in the lift curves. Thus the effect of the gap on C_{L_δ} is no greater than on C_{L_α} for the linear range.

Experimental results are available for the lift on the wing in the presence of the body due to variation in δ. These experimental results are compared with the theoretical results determined from equation (10) in figure 8(d). The flagged points are those points for which the theoretical value of $(C_{L_\alpha})_W$ was used in equation (10) but for which experimental values of $(C_{L_\alpha})_W$ were available. Using the experimental values of $(C_{L_\alpha})_W$ in equation (10) yields the solid points of figure 8(d). The agreement between theory and experiment is considered good, although the theoretical points are generally slightly high.

Pitching-Moment Effectiveness

The factors affecting pitching moment are manifest either through their effects on lift or center of pressure. The adequacy of the present method for determining lift has already been discussed, and the center-of-pressure positions of the complete configuration will now be considered. The center-of-pressure positions of the combination have been calculated for the complete combination as a fraction of the body length behind the body nose by the following equations:

$$\left(\frac{\bar{l}}{l} \right)_{C\alpha} = \left(\frac{\bar{c}}{l} \right) \frac{(C_{m_\alpha})_C}{(C_{L_\alpha})_C} \tag{23}$$

$$\left(\frac{\bar{l}}{l} \right)_{C\delta} = \left(\frac{\bar{c}}{l} \right) \frac{(C_{m_\delta})_C}{(C_{L_\delta})_C} \tag{24}$$

The moments are taken about the body nose in equations (23) and (24). These equations were used for obtaining both the experimental and theoretical values.

<u>Angle of attack.</u>- A comparison of the experimental and theoretical values of $(\bar{l}/l)_{C_\alpha}$ is given in figure 9(a) for a number of wing-body combinations. For the combinations shown, the experimental centers of pressure are on the average about 0.02 l in front of the theoretical positions. In the correlation of experimental and theoretical values of center of pressures for complete combinations with fixed wings and no gap, it was found in reference 6 that the experimental values of the center of pressure were in front of the theoretical values by varying amounts for triangular, rectangular, and trapezoidal wing-body combinations. For triangular combinations the amount was 0.009 l; for rectangular combinations, 0.026 l; and for trapezoidal combinations, 0.017 l. If these corrections are applied to the theoretical values of $(\bar{l}/l)_{C_\alpha}$ as recommended in reference 6, then the average displacement between theory and experiment is reduced as shown by figure 9(b). The present method, in conjunction with the corrections of reference 6, thus gives a means of estimating $(\bar{l}/l)_{C_\alpha}$ to within about ±0.01 l.

<u>Wing deflection angle.</u>- A comparison of the experimental values of $(\bar{l}/l)_{C_\delta}$ with the theoretical values is presented in figure 9(c). The experimental results are again slightly forward of the theoretical results by about 0.02 l. The correction mentioned in connection with angle of attack brings the experimental and theoretical values into even better accord as shown by figure 9(d). Thus the present method, in conjunction with the corrections of reference 6, gives a means of estimating $(\bar{l}/l)_{C_\delta}$ to within about ±0.01 l.

Hinge-Moment Coefficient

The hinge moments of an all-movable wing depend on the lift developed by the wing in the presence of the body as well as the center-of-pressure position of the wing. While a given percentage error in determining the value of $(C_L)_{W(B)}$ causes the same percentage error in C_h, the same cannot be said for center-of-pressure position. Consider an all-movable wing with the center of pressure displaced 5 percent of the mean aerodynamic chord from the hinge line. An error of 1 percent of the mean aerodynamic chord in center-of-pressure position causes an error of 20 percent in hinge-moment coefficient. The necessity of having accurate estimates of center-of-pressure position to obtain accurate hinge-moment estimates is thus apparent. Furthermore, any effects such as Reynolds number, airfoil section, or slight wind-tunnel flow irregularities which would otherwise be inconsequential may well have important effects on hinge moments. In the ensuing comparison between theoretical and experimental values of $(\bar{x}/c_r)_{W(B)}$ these facts should be kept in mind.

Triangular wing and body combinations.- An analysis of the data of
table I reveals that most of the available hinge-moment data are for
triangular wing and body combinations with an r/s ratio of 0.216.
The experimental values of $(\bar{x}/c_r)_{W(B)\alpha}$ are compared with the theoreti-
cal values in figure 10 as a function of βA for constant r/s.
Considering first the experimental points, these have been marked with
their identifying numbers from table I. Some differences in $(\bar{x}/c_r)_{W(B)\alpha}$
are shown between data from different tunnels at the same value of βA.
The data all illustrate a rearward shift of center of pressure with
increase in βA. For purposes of comparison, the wing-alone center-of-
pressure locations are shown for three of the experimental points.

The theoretical values of $(\bar{x}/c_r)_{W(B)\alpha}$ determined from slender-body
theory (fig. 4) are shown in figure 10. The line representing the theory
is shown solid for low values of βA for which it is directly applicable,
and has been extended dotted to higher values of βA. Also included in
the figure is the value of $(\bar{x}/c_r)_W$ as given by linear theory (or
slender-body theory), which is valid for all values of βA. It is clear
that the experimental values of $(\bar{x}/c_r)_W$ and $(\bar{x}/c_r)_{W(B)\alpha}$ are forward of
their theoretical values. However, they are forward of their respective
theoretical values by about the same amount for the same value of βA.
This means that the difference between $(\bar{x}/c_r)_W$ and $(\bar{x}/c_r)_{W(B)\alpha}$, which
represents the interference, is given fairly well by the theory. There-
fore the most accurate method of obtaining the theoretical value of
$(\bar{x}/c_r)_{W(B)\alpha}$ would be to add to the measured value of $(\bar{x}/c_r)_W$ the
theoretical difference between $(\bar{x}/c_r)_{W(B)\alpha}$ and $(\bar{x}/c_r)_W$. Although suf-
ficient data are not available to make a thorough check on the validity
of this procedure, the desirability of knowing the experimental wing-
alone characteristics is clear.

A plot of the experimental values of $(\bar{x}/c_r)_{W(B)\delta}$ against βA for
the triangular wing and body combination of $r/s = 0.216$ is presented
in figure 11. The experimental data differ by about 0.005 in $(\bar{x}/c_r)_{W(B)\delta}$
for $r/s = 0.216$. Some other data for $r/s = 0.200$ show centers of
pressure about 2 percent forward of the $r/s = 0.216$ results for some
unknown reason. Wing-alone center-of-pressure positions are shown for
three of the combinations. The differences between the experimental
values of $(\bar{x}/c_r)_W$ and $(\bar{x}/c_r)_{W(B)\delta}$ are not very large so that the inter-
ference effects are small, as indeed theory indicates. However, it is
noted that the experimental center-of-pressure positions for the wing
in the presence of the body are shifted considerably forward of the

theoretical position. Most of this shift is explained by the difference between the theoretical and experimental wing-alone results as shown by the figure. Again, the procedure suggested in connection with $(\bar{x}/c_r)_{W(B)\alpha}$ would give good values of $(\bar{x}/c_r)_{W(B)\delta}$ also.

Some insight into the relative positions of the wing centers of pressure due to angle of attack and wing deflection angle is given in figure 12. The difference between the two quantities as given by the theoretical results of figure 4 is plotted as a function of r/s in figure 12. The available experimental data from the table are included in the figure. Considering the small differences involved, the agreement between experiment and theory is considered satisfactory.

Rectangular wing and body combinations.- The theoretical and experimental information available for rectangular wing and body combinations is much less than that available for triangular wing and body combinations as the table shows. No theoretical results for $(\bar{x}/c_r)_{W(B)\alpha}$ are available, and while the method of reference 4 is adapted to their determination, the necessary calculations were not carried out. Reference 4, however, does give the theoretical values of $(\bar{x}/c_r)_{W(B)\delta}$ and the results have already been given in figure 6. These results have been plotted as a function of βA for $r/s = 0.216$ and $\beta A \geq 2$ in figure 13. The theoretical curve has also been extrapolated toward $\beta A = 0$. Included in figure 13 are two experimental points for low values of βA. They are in good accord with the extrapolation of the theory. Figure 13 shows that the change in the center of pressure of a rectangular all-movable control is large for significant changes in βA. Since the center-of-pressure travel is large compared to the deviation between experiment and theory, the theoretical results may be sufficiently accurate for predicting hinge moments. However, before a satisfactory method for predicting hinge moments of rectangular all-movable wings is developed that will account for both angle of attack and wing deflection angle, further theoretical and experimental work must be performed.

CONCLUSIONS

A simple method has been advanced for estimating lift, pitching-moment, and hinge-moment characteristics of all-movable wings in the presence of the body as well as the characteristics of wing-body combinations employing such wings. By comparing experimental values for the

NACA RM A52D29

ranges of angle of attack and wing deflection angle for which the characteristics are linear with the theoretical values estimated by the present method, the following conclusions have been drawn:

1. The theoretical and experimental values of the lift quantities $(C_{L_\alpha})_C$ and $(C_{L_\alpha})_{W(B)}$ were in good accord. The theoretical values of $(C_{L_\delta})_C$ and $(C_{L_\delta})_{W(B)}$ exhibited a tendency to be larger than the corresponding experimental values for reasons unknown.

2. The center-of-pressure positions for the wing-body combinations, $(\bar{l}/l)_\alpha$ and $(\bar{l}/l)_\delta$, were given to within about ± 0.01 l by the present method.

3. For moderate gap sizes and for the ranges of angle of attack and wing deflection angle for which the characteristics are linear, an all-movable wing acts aerodynamically as if no gap exists between the wing and body.

4. Accurate values of the hinge-moment coefficient are not predicted by the present method for triangular controls. An accurate estimate of hinge-moment coefficient can probably be obtained by adding to the experimental center-of-pressure positions of the wing alone the theoretical shifts due to interference as determined by the present method. More experimental data are needed to prove this proposed empirical procedure conclusively.

5. Although the empirical procedure suggested in the present report should be adequate for estimating the hinge moments of rectangular controls, more theoretical and experimental work is required before the hinge moments of rectangular controls can be predicted with certainty.

Ames Aeronautical Laboratory,
    National Advisory Committee for Aeronautics,
        Moffett Field, Calif.

APPENDIX

WING—PANEL CENTER OF PRESSURE DUE TO DEFLECTING

WINGS OF WING AND BODY COMBINATIONS

In reference 8 Spreiter has given the loading and center-of-pressure positions for the wing of a wing and body combination with zero wing incidence. However, for all-movable controls the problem of the center of pressure of the wing in the deflected state with the body at zero angle of attack is of importance. This result is readily obtained by methods similar to those used by Spreiter. In fact, the wing loading, available from some unpublished work of Gaynor J. Adams of the Ames Aeronautical Laboratory, is given as

$$\left(\frac{\Delta p}{q\delta}\right)_W = \frac{2 \tan \epsilon \ (\eta^4 - r^4) \left(\pi + \cos^{-1} \frac{2r}{\eta + r^2/\eta}\right)}{\pi \eta^3 \sqrt{(\eta + r^2/\eta)^2 - (y + r^2/y)^2}} \qquad (A1)$$

wherein the symbols are defined in figure 14. If M_W is the moment developed by both wing panels about the y axis, it is readily shown that this moment is given by

$$\frac{M_W}{q\delta} = 2 \int_r^s \frac{\eta}{\tan \epsilon} \int_r^\eta \left(\frac{\Delta p}{q\delta}\right)_W dy \frac{d\eta}{\tan \epsilon} \qquad (A2)$$

One integration yields the result

$$\frac{M_W}{q\delta} = \frac{1}{\pi \tan \epsilon} \int_r^s \frac{(\eta^4 - r^4)}{\eta^2} \left(\pi + 2 \cos^{-1} \frac{2r \ \eta}{\eta^2 + r^2}\right)^2 d\eta \qquad (A3)$$

The second integration caused some difficulty since the integrals could not be expressed in terms of tabulated functions. Instead it was found necessary to introduce two functions defined by the following rapidly convergent series:

$$\chi (x) = x + \frac{1}{2} \left(\frac{x^3}{3^2}\right) + \frac{1 \cdot 3}{2 \cdot 4} \left(\frac{x^5}{5^2}\right) + \frac{1 \cdot 3 \cdot 5}{2 \cdot 4 \cdot 6} \left(\frac{x^7}{7^2}\right) + \cdots \qquad (A4)$$

$$\psi (x) = x - \frac{x^3}{3^2} + \frac{x^5}{5^2} - \frac{x^7}{7^2} + \cdots \qquad (A5)$$

In terms of these functions, the moment is given by

$$\frac{\pi \tan \epsilon}{q\delta} M_W = \frac{16(s^4 + 3r^4)}{3s}(\tan^{-1} s/r)^2 - \frac{16r}{3}(s^2 + r^2) \tan^{-1} s/r -$$

$$\frac{4\pi^2 r^3}{3} + \frac{16r^3}{3}(s - r) + \frac{8\pi r^3}{3} - 16\pi r^3 \log(s/r) +$$

$$\frac{32\pi r^3}{3} \log \frac{s^2 + r^2}{2r^2} - 32r^3 \left[\psi(r/s) - \psi(1)\right] -$$

$$\frac{128 r^3}{3} \left[\chi(1/\sqrt{2}) - \chi(r/\sqrt{s^2 + r^2})\right] \tag{A6}$$

If the moment is divided by the lift of the exposed wing panels as given in terms of $k_{W(B)}$ (equation (11)), the moment arm will be obtained. It is convenient to express this moment arm in fractions of the root chord behind the leading edge of the wing-body juncture in the following equation wherein τ is the radius-semispan ratio:

$$\left(\frac{\bar{x}}{c_r}\right)_{W(B)\delta} = \frac{1}{2\pi k_W (1 - \tau)^3} \left\{ \frac{16(1 + 3\tau^4)}{3}\left(\tan^{-1}\frac{1}{\tau}\right)^2 - \right.$$

$$\frac{16\tau}{3}(1 + \tau^2)\tan^{-1}\frac{1}{\tau} - \frac{4\pi^2\tau^3}{3} + \frac{16\tau^2}{3}(1-\lambda) + \frac{8\pi\tau^3}{3} + 16\pi\tau^3 \log \tau +$$

$$\frac{32\pi\tau^3}{3} \log \frac{1 + \tau^2}{2\tau^2} - 32\tau^3\left[\psi(\tau) - \psi(1)\right] - \frac{128\tau^3}{3}\left[\chi(1/\sqrt{2}) - \right.$$

$$\left.\left.\chi\left(\frac{\tau}{\sqrt{1 + \tau^2}}\right)\right]\right\} - \frac{\tau}{1-\tau} \tag{A7}$$

The quantity $(\bar{x}/c_r)_{W(B)\delta}$ has been plotted as a function of r/s in figure 4.

REFERENCES

1. Conner, D. William: Aerodynamic Characteristics of Two All-Movable Wings Tested in the Presence of a Fuselage at a Mach Number of 1.9. NACA RM L8H04, 1948.

2. Stone, David G.: Comparisons of the Effectiveness and Hinge Moments of All-Movable Delta and Flap-Type Controls on Various Wings. NACA RM L51C22, 1951.

3. Nielsen, Jack N., and Kaattari, George E.: Method for Estimating Lift Interference of Wing-Body Combinations at Supersonic Speeds. NACA RM A51J04, 1951.

4. Nielsen, Jack N., and Pitts, William C.: Wing-Body Interference at Supersonic Speeds With an Application to Combinations With Rectangular Wings. NACA TN 2677, 1952.

5. Heaslet, Max. A., and Spreiter, John R.: Reciprocity Relationships in Aerodynamics. NACA TN 2700, 1952.

6. Kaattari, George E., Nielsen, Jack N., and Pitts, William C.: Method for Estimating Moment Interference of Wing-Body Combinations at Supersonic Speeds. NACA RM A52B06, 1952.

7. Lomax, Harvard, and Byrd, Paul F.: Theoretical Aerodynamic Characteristics of a Family of Slender Wing-Tail-Body Combinations. NACA TN 2554, 1951.

8. Spreiter, John R.: The Aerodynamic Forces on Slender Plane- and Cruciform-Wing and Body Combinations. NACA Rep. 962, 1950. (Formerly NACA TN's 1662 and 1897)

9. Peters, R. G.: Data Report for Supersonic Wind Tunnel Tests on GAPA Model FR-87. Fifth Aberdeen Test Period, M = 1.72. Boeing Aircraft Co., D-8397, (Tech. Rept. No. 111-7), Aug. 1947.

10. Peters, R. G.: Data Report for Supersonic Wind Tunnel Tests on GAPA FR-87. Sixth and Seventh Aberdeen Test Periods, M = 1.72 and M = 1.28. Boeing Aircraft Company, D-8788, (Tech. Rept. No. 111-9), Feb. 1948.

11. Jevon, R. W.: Data Report for Supersonic Wind Tunnel Tests on XSSM-N-6 Models #3B and #4A. 2nd - 4th Daingerfield Test Periods, M = 2.0, 2.25, 1.73. Grumman Aircraft Engineering Corp., Rept. No. P/A 3141.20, Sept. 1949.

████████████

12. Jevon, R. W., and Bastedo, W., Jr.: Data Report for Supersonic
     Wind-Tunnel Tests on XSSM-N-6 Model #3A. First Daingerfield Test
     Period, M = 2.0. Grumman Aircraft Engineering Corp., Rept. No.
     P/A 3128.20, Apr. 1949.

13. Jevon, R. W.: Data Report for Supersonic Wind Tunnel Tests on
     XSSM-N-6 Models #3C and #6A. Fifth Daingerfield Test Period,
     M = 2.0. Grumman Aircraft Engineering Corp., Rept. No. 3147.20,
     Mar. 1950.

14. Stivers, Louis S., Jr., and Malick, Alexander W.: Wind-Tunnel
     Investigation at Mach Numbers from 0.50 to 1.29 of an All-Movable
     Triangular Wing of Aspect Ratio 4 Alone and with a Body.
     NACA RM A9L01, 1950.

15. Delameter, H. D., Stamper, J. C., and Solvason, J. C.:
     Model XAAM-N-2. Preliminary Analysis of Force and Moment
     Characteristics from Supersonic Wind Tunnel Tests of a
     45-Percent-Scale Semi-Span Model. Ballistic Res. Lab.,
     Aberdeen Proving Ground, Maryland, Mach No. 1.72. Douglas Air-
     craft Co., Inc., Rept. No. SM-13469, Oct. 20, 1949.

16. Clark, J. M., Jr.: Wind-Tunnel Tests of a Forty-Five-Percent Scale
     Semi-Span XAAM-N-2 Model at M = 2.00 and M = 1.50. Consolidated
     Vultee Aircraft Corp., OAL Repts. 185 and 185-1, Sept. 1949.

17. Ellis, Macon C., Jr., and Grigsby, Carl E.: Aerodynamic Investiga-
     tion at Mach Number 1.92 of a Rectangular Wing and Tail and Body
     Configuration and Its Components. NACA RM L9L28a, 1950.

18. Wood, H. T., Jr.: Stability and Control Tests of a 1/12-Scale
     STV-3 Model at Mach Numbers 1.50 and 2.00 in the 19 × 27.5 Inch
     Wind Tunnel for the Johns Hopkins University. Consolidated Vultee
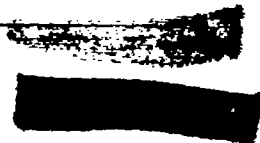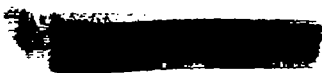   Aircraft Corp., OAL Rept. 99, July 1948.

TABLE I.- SUMMARY OF AERODYNAMIC AND GEOMETRIC
CHARACTERISTICS AND TEST CONDITIONS FOR
ALL-MOVABLE WING AND BODY COMBINATIONS

No.	Sketch	M_0	R	Wing section	δ (in.)	g (in.)	βA	λ	$\Lambda_{L.E.}$	$\frac{r}{s}$	r (in.)	l (in.)	l_a (in.)	l_f (in.)	Reference	Facility
1		1.72	1.05×10^6	¹hex.	2.49	---	1.87	0.130	60	0.265	0.50	12.00	2.04	6.28	9	Aberdeen
2		1.72	$.80\times10^6$	hex.	1.90	---	2.80	.253	50	.228	.50	12.00	5.61	3.68	9	Aberdeen
3		1.28	1.05×10^6	hex.	2.49	---	1.07	.130	60	.265	.50	12.00	4.97	3.35	10	Aberdeen
4		1.28	$.80\times10^6$	hex.	1.90	---	1.60	.253	50	.228	.50	12.00	5.61	3.68	10	Aberdeen
5		1.73	$.42\times10^6$	²d.w.	.77	---	3.77	.500	26.6	.486	1.00	22.97	18.55	3.43	11	Daingerfield
6		2.25	$.52\times10^6$	d.w.	.77	---	5.38	.500	26.6	.486	1.00	22.97	18.55	3.43	11	Daingerfield
7		2.00	1.27×10^6	hex.	2.12	---	5.11	.461	14	.250	1.00	22.97	5.90	14.49	12	Daingerfield
8		2.00	$.56\times10^6$	d.w.	.94	---	4.62	.500	26.6	.437	1.00	22.97	18.45	3.32	13	Daingerfield
9		2.00	$.46\times10^6$	d.w.	.77	---	4.62	.500	26.6	.486	1.00	22.97	18.55	3.43	13	Daingerfield
10		2.07	$.64\times10^6$	d.w.	1.50	0.005	7.25	0	45	.200	.56	10.5	4.50	3.75	-	Ames 1×3
11		1.20	1.09×10^6	d.w.	3.33	.03	2.65	0	45	.200	1.25	30.00	15.00	10.00	14	Ames 1×3-1/2
12		1.24	1.09×10^6	d.w.	3.33	.03	2.93	0	45	.200	1.25	30.00	15.00	10.00	14	Ames 1×3-1/2
13		1.29	1.09×10^6	d.w.	3.33	.03	3.26	0	45	.200	1.25	30.00	15.00	10.00	14	Ames 1×3-1/2
14		1.72	3.92×10^6	d.w.	7.54	---	3.24	0	60	.216	1.80	29.00	5.14	12.55	15	Aberdeen
15		1.50	3.98×10^6	d.w.	7.54	.014	2.58	0	60	.216	1.80	29.00	5.14	12.55	16	Daingerfield
16		2.00	4.52×10^6	d.w.	7.54	.014	4.00	0	60	.216	1.80	29.00	5.14	12.55	16	Daingerfield
17		1.90	1.9×10^6	³b.c.	2.64	.005	3.74	0	60	.269	.80	19.20	5.63	9.61	1	Langley 9"×12"
18		1.90	1.4×10^6	d.w.	1.87	.005	5.69	0	0	.232	.80	19.20	6.27	10.81	1	Langley 9"×12"
19		1.92	$.2\times10^6$	b.c.	.616	.000	5.13	1	0	.228	.35	8.75	.08	8.05	17	Langley 9"×12"
20		1.15	1.25×10^6	d.w.	7.54	.016	1.31	0	60	.216	1.80	57.31	25.08	20.92	-	Ames 6×6
21		1.20	1.25×10^6	d.w.	7.54	.016	1.53	0	60	.216	1.80	57.31	25.08	20.92	-	Ames 6×6
22		1.30	1.25×10^6	d.w.	7.54	.016	1.92	0	60	.216	1.80	57.31	25.08	20.92	-	Ames 6×6
23		1.40	1.25×10^6	d.w.	7.54	.016	2.27	0	60	.216	1.80	57.31	25.08	20.92	-	Ames 6×6
24		1.53	1.25×10^6	d.w.	7.54	.016	2.68	0	60	.216	1.80	57.31	25.08	20.92	-	Ames 6×6
25		1.70	1.25×10^6	d.w.	7.54	.016	3.18	0	60	.216	1.80	57.31	25.08	20.92	-	Ames 6×6
26		1.90	1.25×10^6	d.w.	7.54	.016	3.74	0	60	.216	1.80	57.31	25.08	20.92	-	Ames 6×6
27		1.40	1.25×10^6	d.w.	7.54	.016	2.27	0	0	.216	1.80	57.31	22.37	23.63	-	Ames 6×6
28		1.90	1.25×10^6	d.w.	7.54	.016	3.74	0	0	.216	1.80	57.31	22.37	23.63	-	Ames 6×6
29		1.40	1.51×10^6	d.w.	11.31	.016	1.13	1	0	.216	1.80	57.31	23.72	22.28	-	Ames 6×6
30		1.90	1.51×10^6	d.w.	11.31	.016	1.87	1	0	.216	1.80	57.31	23.72	22.28	-	Ames 6×6
31		2.0	----	hex.	---	---	5.84	0	22	.286	.56	12.5	4.65	6.44	18	Daingerfield
32		1.5	----	hex.	---	---	3.77	0	22	.286	.56	12.5	4.65	6.44	18	Daingerfield

¹hex. indicates hexagonal
²d.w. indicates double wedge
³b.c. indicates biconvex

TABLE I.- CONCLUDED
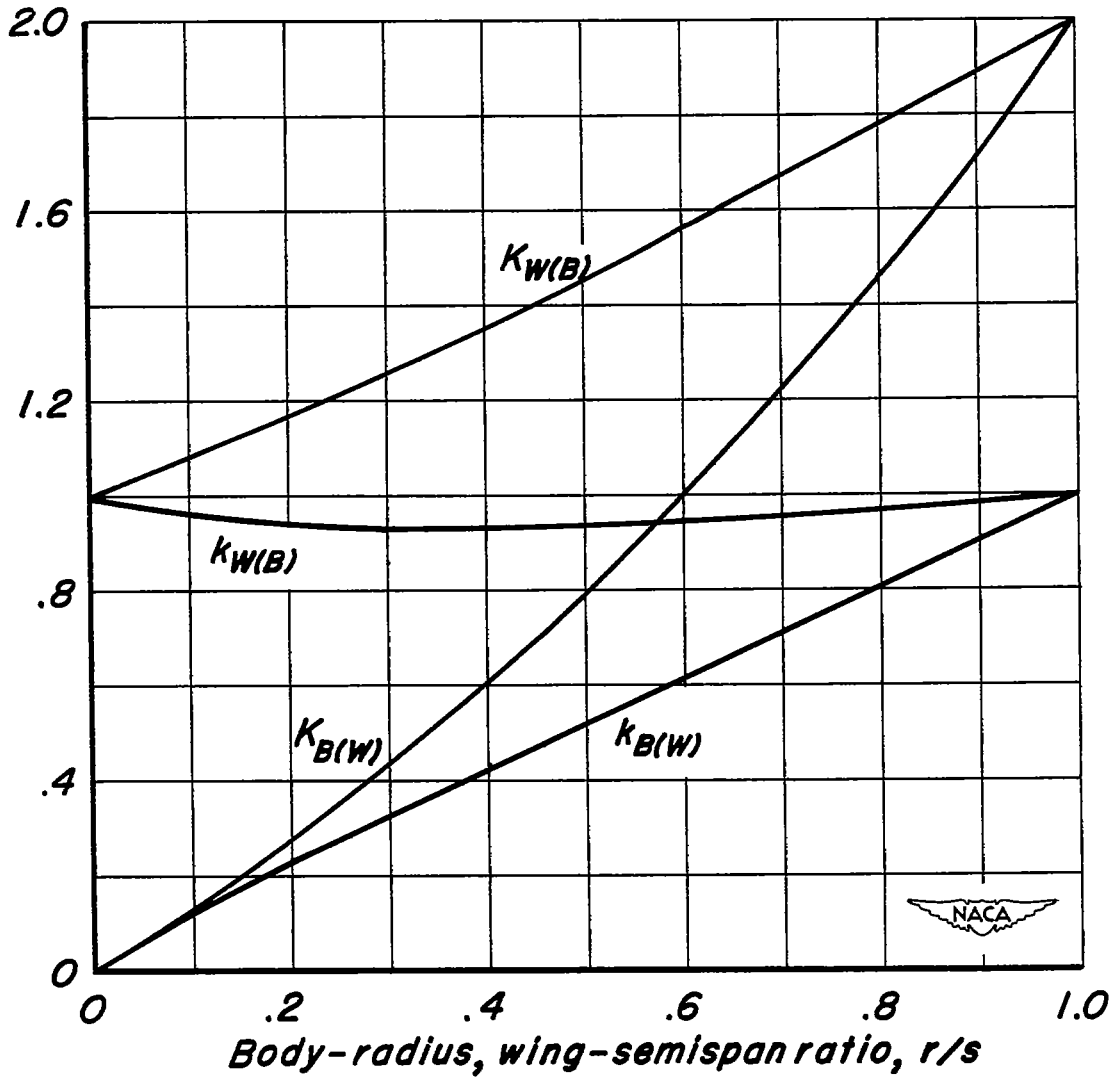

*Numbers in parentheses are theoretical values.

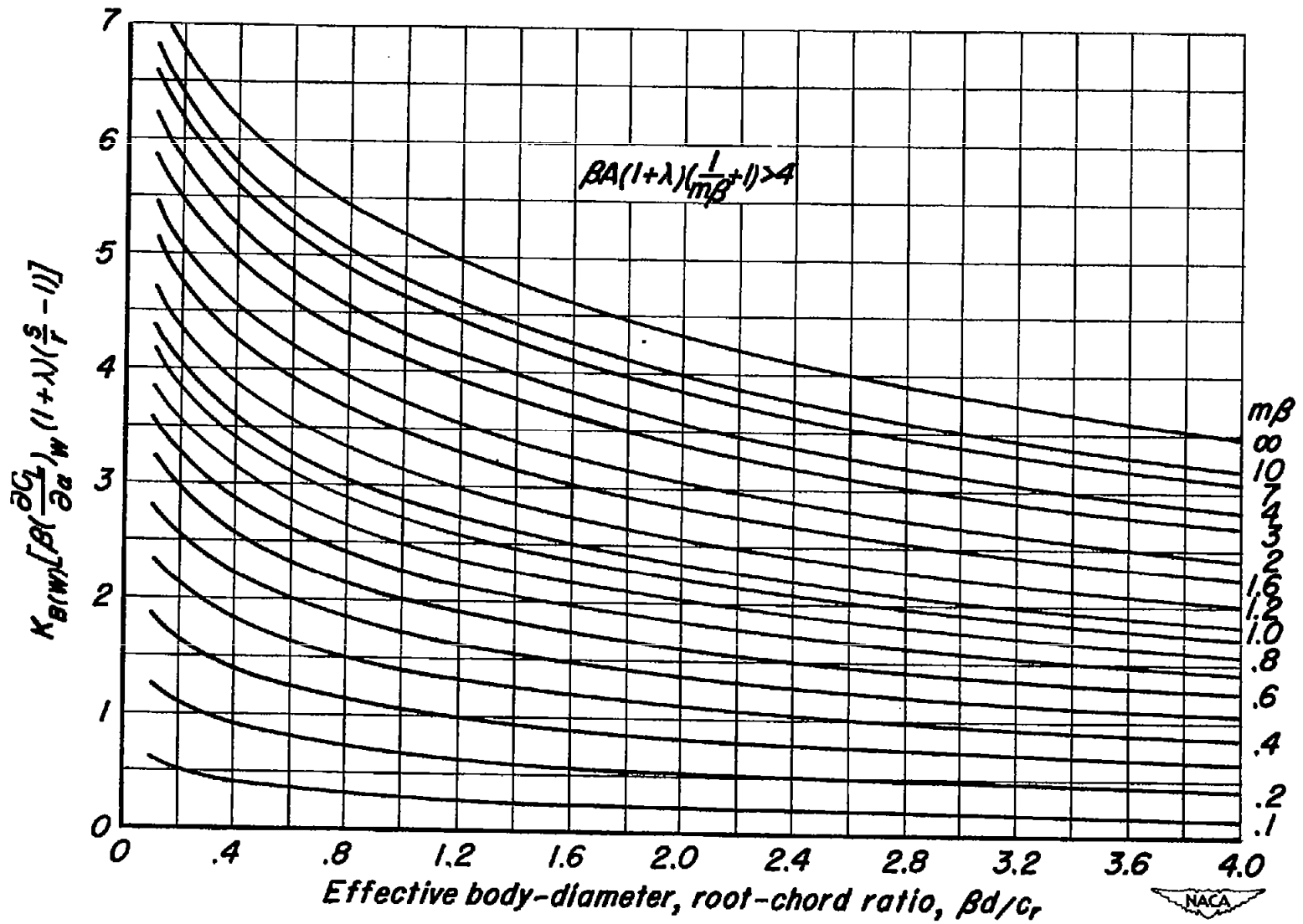Figure 1.- Values of $K_{W(B)}$, $K_{B(W)}$, $k_{W(B)}$, and $k_{B(W)}$ from slender-body theory.

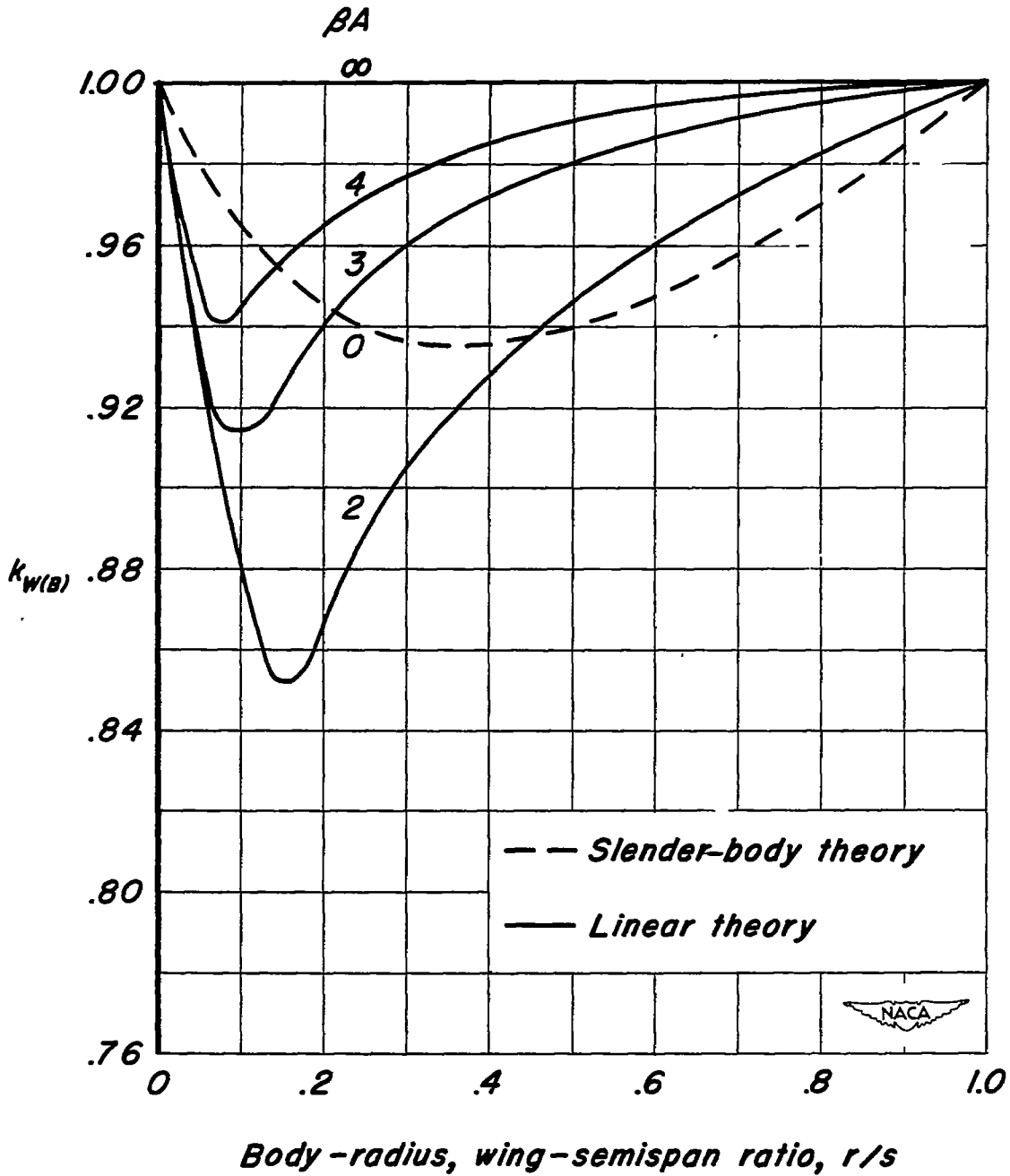Figure 2.- Design chart for determination of $K_{B(W)}$.

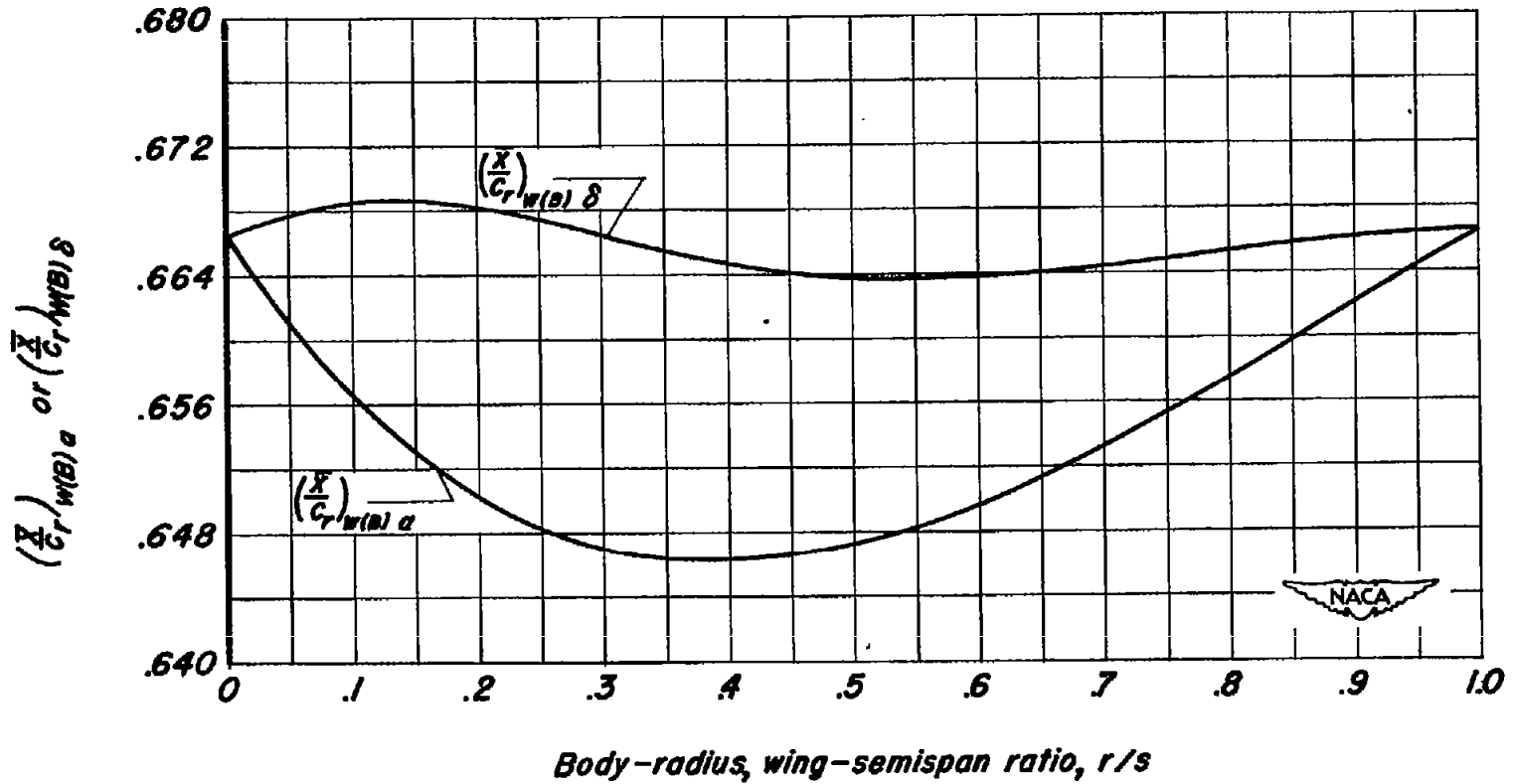Figure 3.—Values of $k_{W(B)}$ for rectangular wing and body combinations.

Figure 4.—Center of pressure of lift acting on wing panel of triangular wing and body combination from slender-body theory.
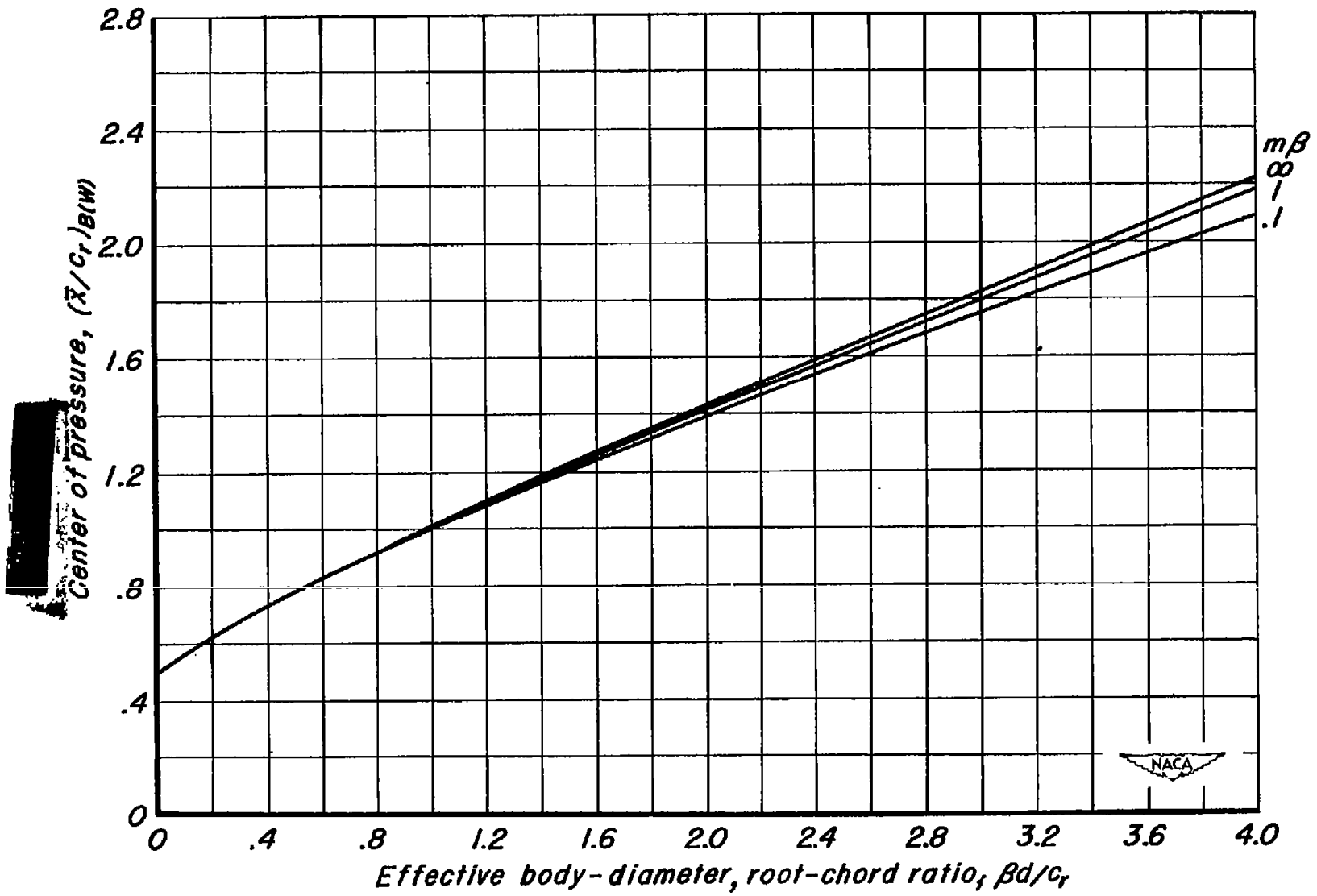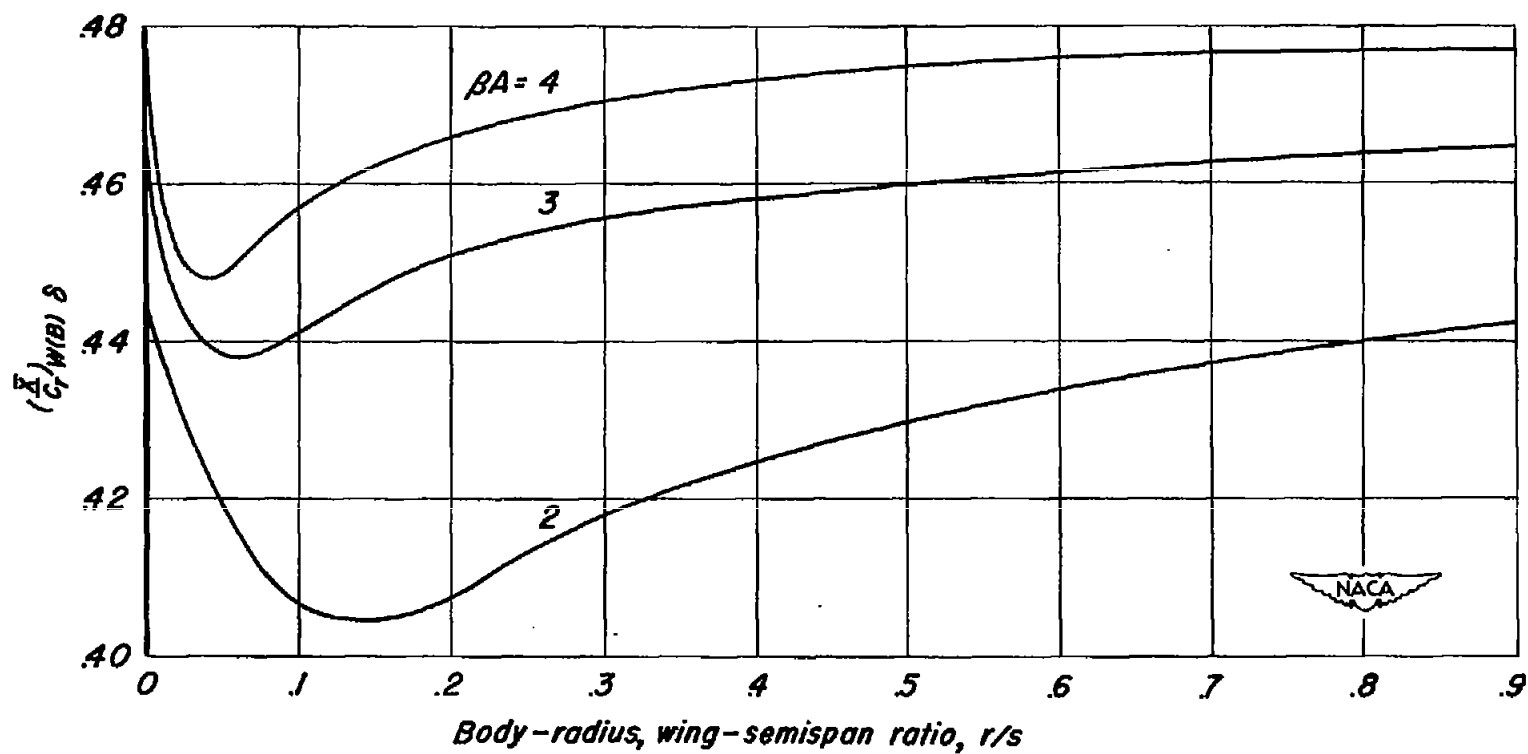
Figure 5.— Design chart for determination of $(\bar{x}/c_r)_{B(W)}$

Figure 6.—Values of $\left(\frac{\bar{X}}{C_r}\right)_{W(B)\,\delta}$ from linear theory for rectangular wing and body combinations.
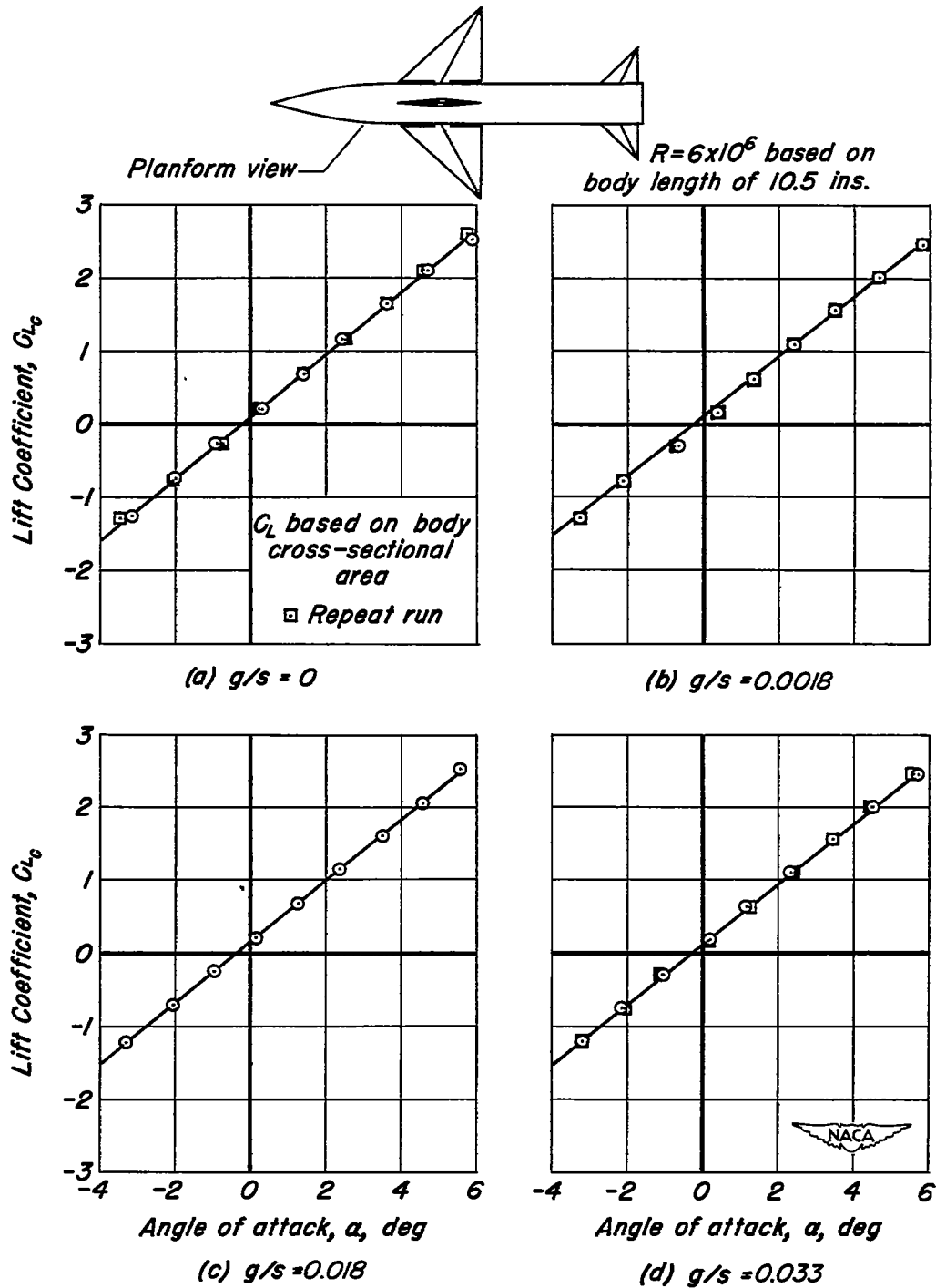
Figure 7.—Effect of gap on the lift characteristics of a triangular wing, body, and tail combination at M = 2.00.

(a) Combination, α

(b) Wing in presence of body, α

(c) Combination, δ

(d) Wing in presence of body, δ
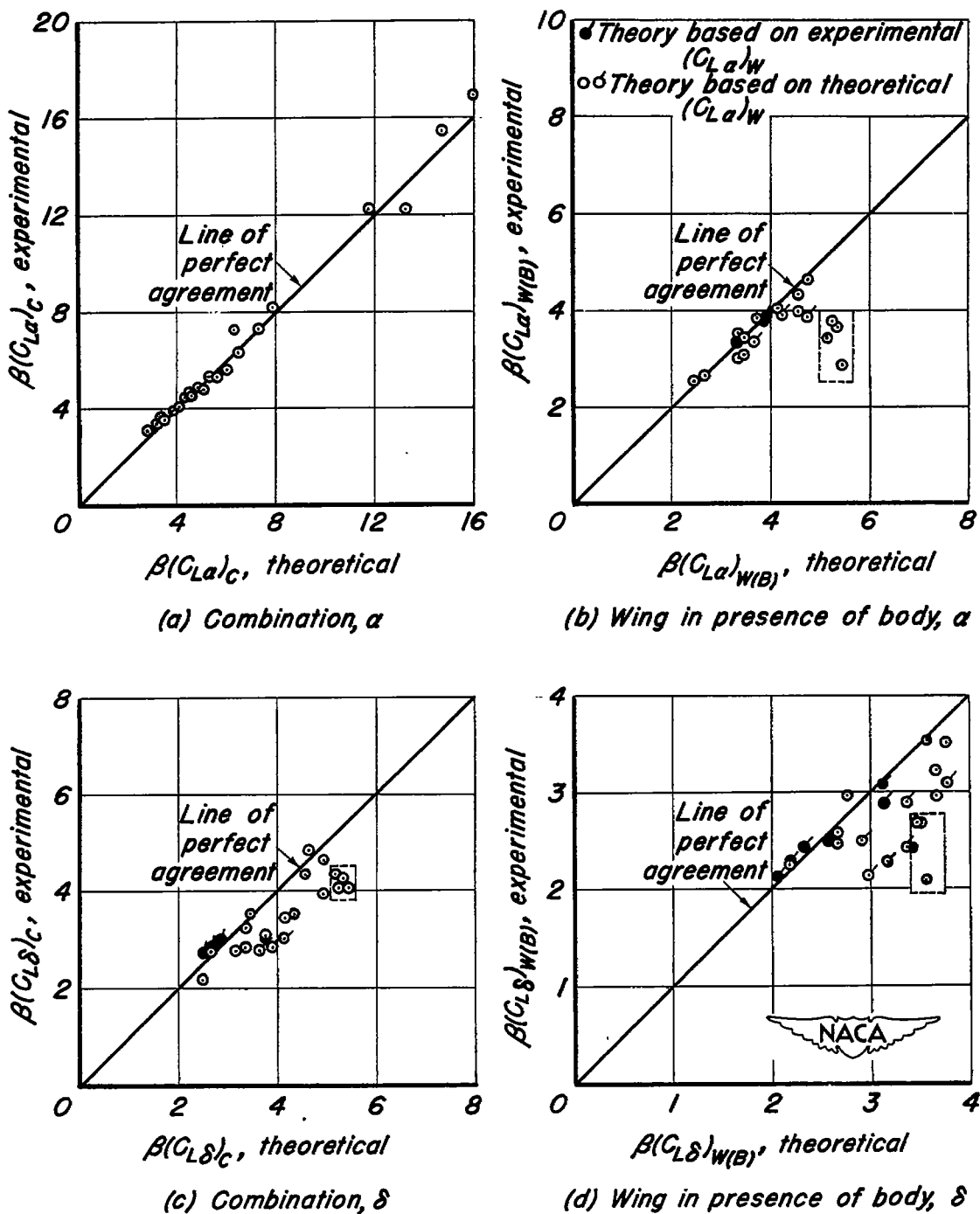
Figure. 8.— Comparison of experimental and theoretical lift-curve slopes for wing-body combinations and for wings in the presence of the body.

(a) Angle of attack, no correction.

(b) Angle of attack, correction applied.

(c) Wing deflection angle, no correction.

(d) Wing deflection angle, correction applied.
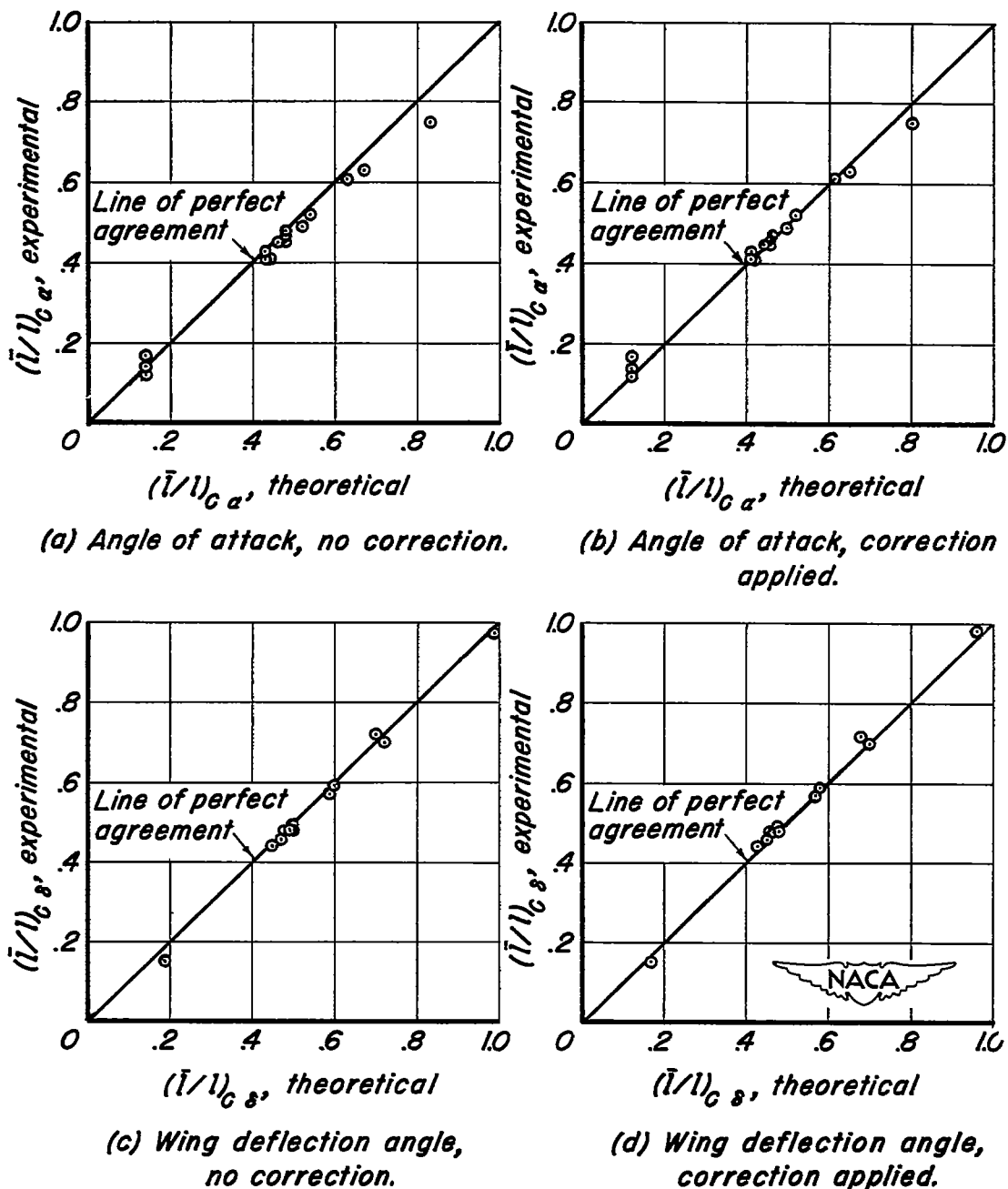
Figure 9.- Comparison between experimental and theoretical center-of-pressure positions for complete wing-body combinations.
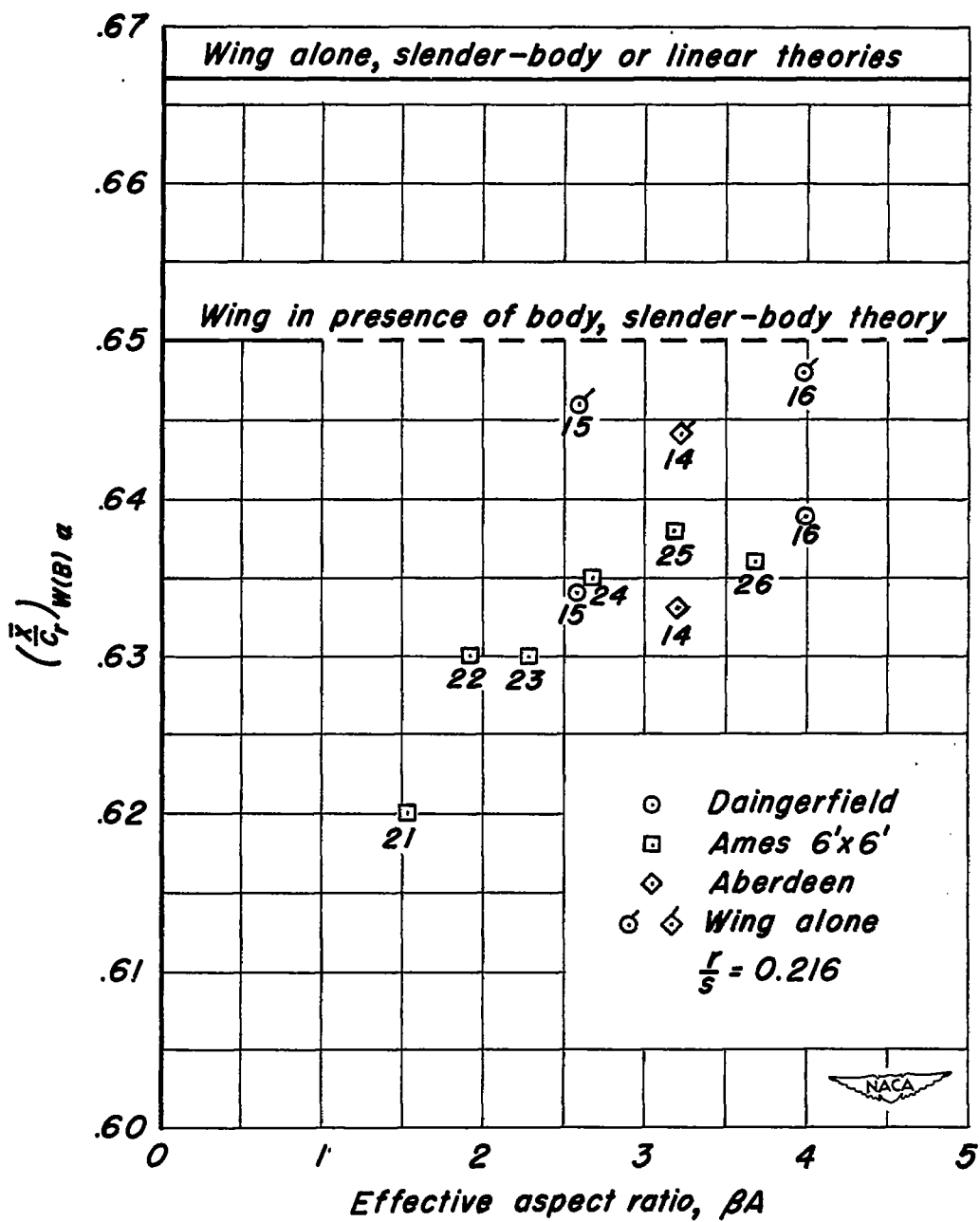
Figure 10.-Comparison between theoretical and experimental values
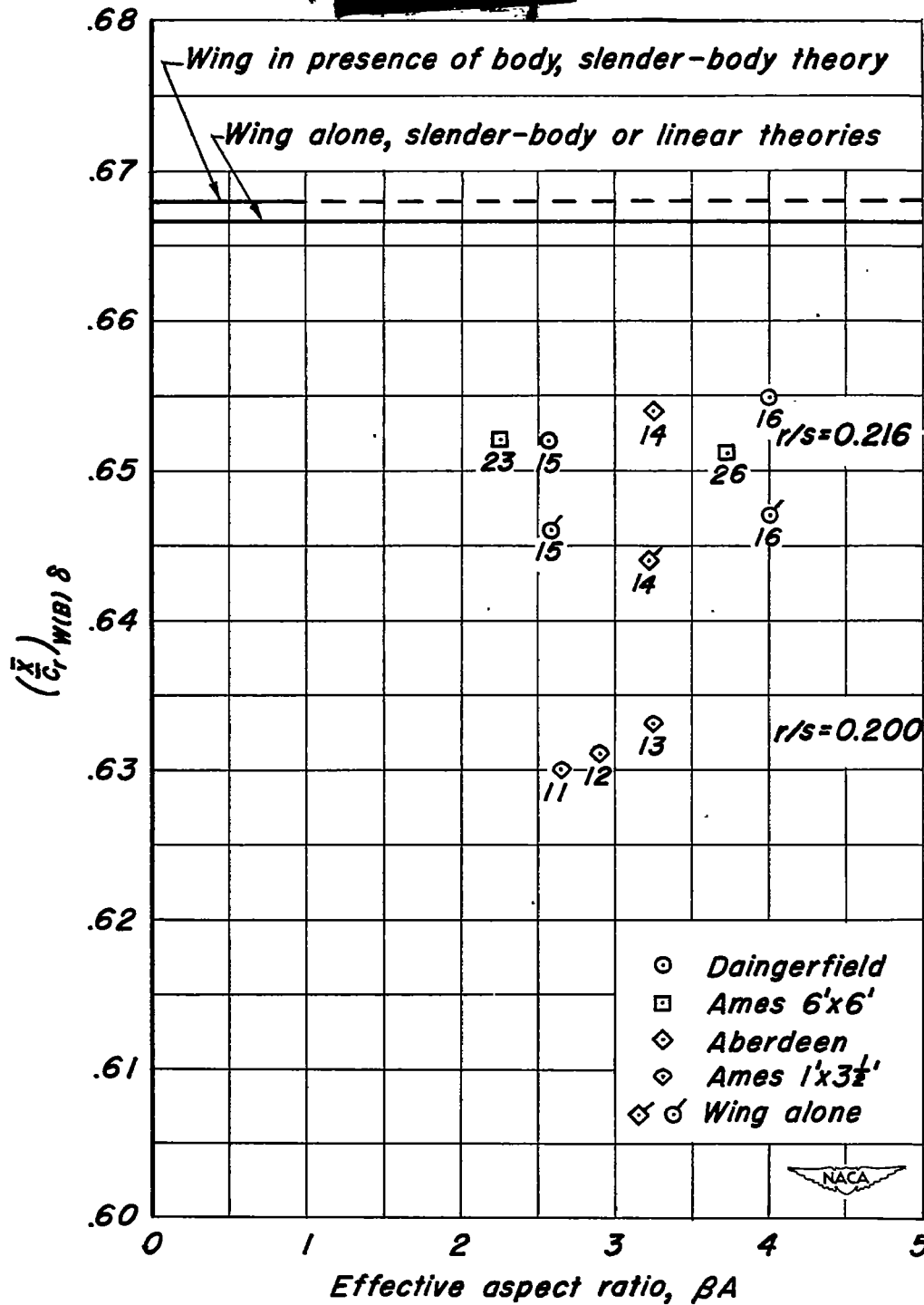
of $\left(\dfrac{\bar{x}}{c_r}\right)_{W(B)\,\alpha}$.

Figure // , - Comparison between theoretical and experimental values of $\left(\frac{\bar{x}}{c_r}\right)_{W(B)\,\delta}$.
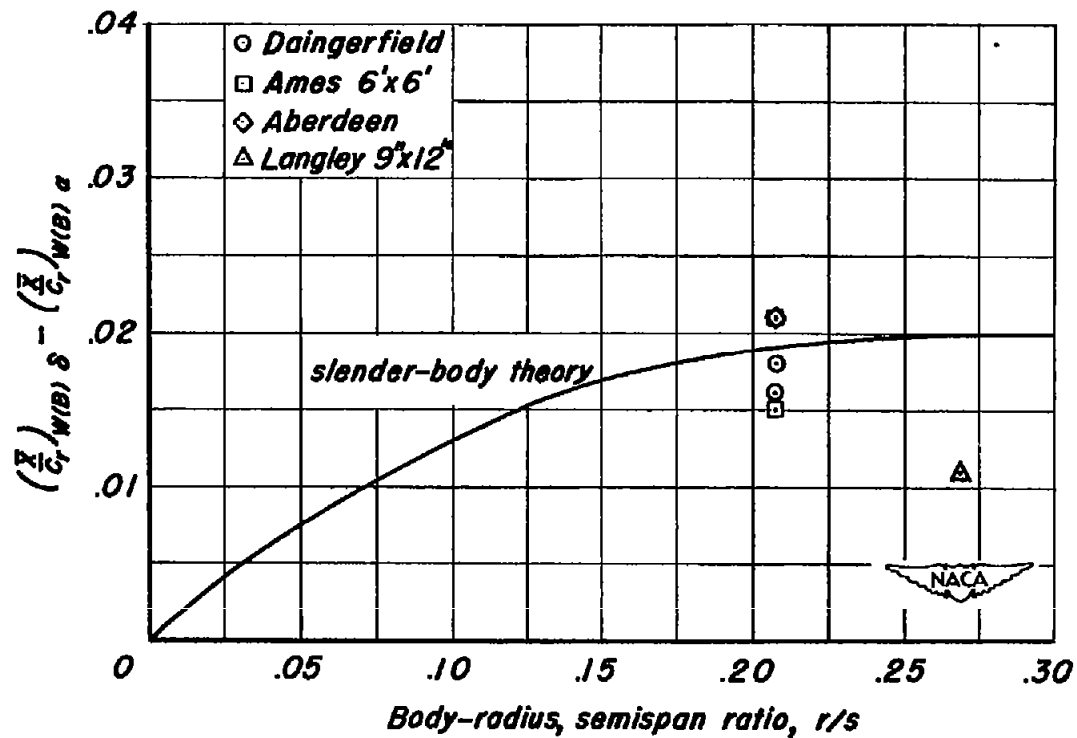
Figure 12.– Comparison between theoretical and experimental differences of $\left(\frac{\bar{x}}{c_r}\right)_{W(B)\,\delta}$ and $\left(\frac{\bar{x}}{c_r}\right)_{W(B)\,\alpha}$ for triangular wing and body combinations.
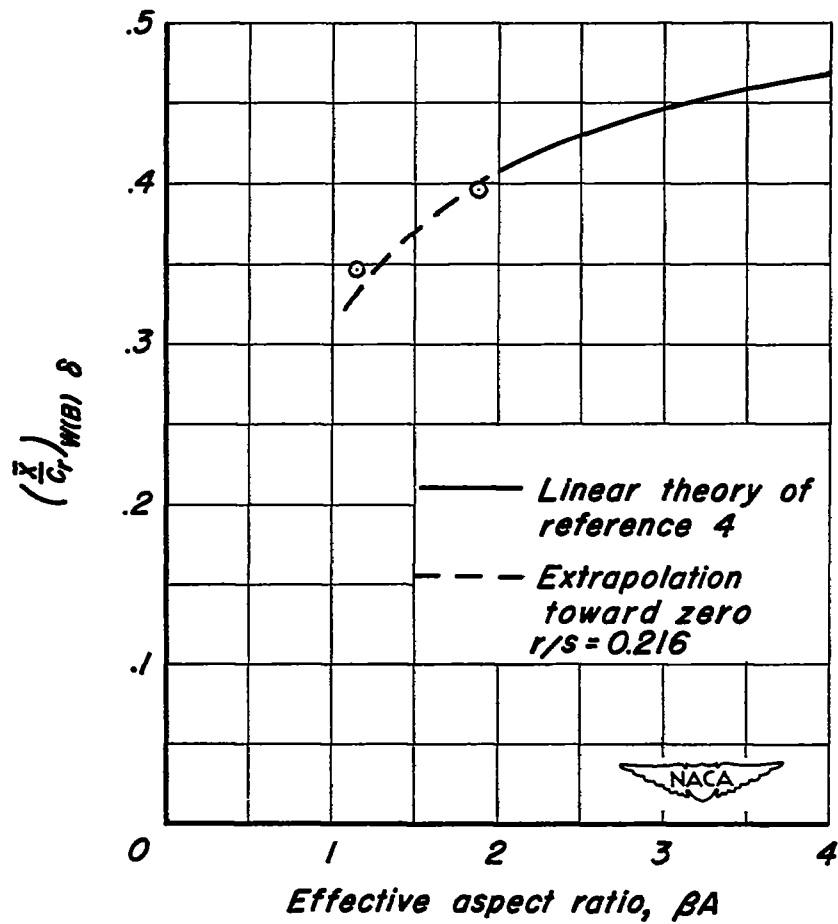
Figure 13.- Comparison between theoretical and experimental values of $\left(\frac{\bar{x}}{c_r}\right)_{W(B)\,\delta}$ for rectangular wing and body combinations.
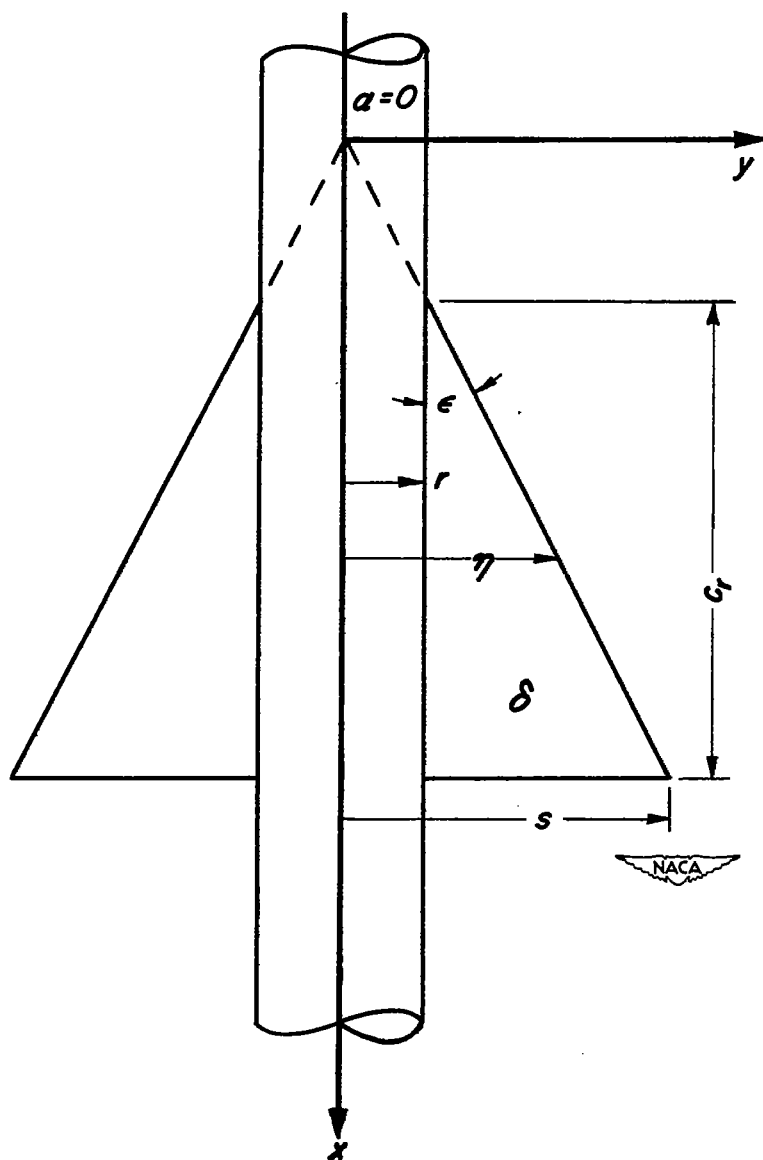
Figure 14.- Coordinate system and symbols for determination of center of pressure due to wing deflection angle.